batteries

MDPI

Article

Research on Aging Evolution and Safety Characteristics of Lithium-Ion Batteries Cycling at Low Temperature

Ruiheng Wang [1] and Bing Xue [2,*]

[1] School of Safety Science and Engineering, Changzhou University, Changzhou 213164, China
[2] Jiangsu Key Laboratory of Advanced Catalytic Materials and Technology, School of Petrochemical Engineering, Changzhou University, Changzhou 213164, China
* Correspondence: xuebing@cczu.edu.cn

Abstract

Complex operating conditions, such as low temperature, can affect the degradation and safety stability of lithium-ion batteries (LIBs). This paper conducts research on the aging evolution and safety characteristics of LIBs under low-temperature conditions (−20 °C), to reveal the change laws of battery degradation and the trends of thermal parameters of aging LIBs. Cycling and charging/discharging experiments under low temperatures were conducted to collect realistic battery data. Various factors such as temperature, cycle number, charging/discharging rate, and depth of discharge/charge (DOD/DOC) are taken into consideration to test the battery cycling and thermal performance. With collected experimental results, basic electrical states of LIBs such as open-circuit voltage (OCV), internal resistance, and capacity are presented. Then, the capacity loss and internal resistance growth are also described and analyzed under various charge/discharge rates and DODs/DOCs. The experimental results show that low temperatures cause an almost 30% increase in polarization resistance, with nonlinear changes in total internal resistance. Moreover, the battery capacity and internal resistance also have extreme points with different charge/discharge rates under −20 °C, which may demonstrate that the charge/discharge rates of LIBs can be optimized under low temperature. Thermal runaway (TR) experiments were also conducted, and the self-heating rate and other indices are presented to show that an aging battery under low temperature still holds large energy to develop TR. The aging trends of LIBs under low temperatures are summarized, and battery safety is clarified to provide a reference for battery lifetime and safety management under low-temperature conditions.

Keywords: lithium-ion batteries; low-temperature conditions; battery degradation; thermal characteristics; safety management

Academic Editor: Pascal Venet

Received: 11 August 2025
Revised: 23 September 2025
Accepted: 14 October 2025
Published: 27 October 2025

Citation: Wang, R.; Xue, B. Research on Aging Evolution and Safety Characteristics of Lithium-Ion Batteries Cycling at Low Temperature. *Batteries* **2025**, *11*, 396. https://doi.org/10.3390/batteries11110396

1. Introduction

Lithium-ion batteries (LIBs) have been widely used as energy supplies for electric vehicles (EVs), energy storage systems (ESSs), and other transportation tools. LIBs always work under the complex operating conditions of different applications [1,2]. The main duty of a battery management system (BMS) is to monitor the real-time states, lifetime, and safety of LIBs. Due to the electrochemical characteristics of LIBs, the input of an LIB is the charging or discharging current, which directly influences its states, lifetime, and safety [3,4]. Besides current input, the ambient temperature of a working battery is another vital factor influencing the activation of lithium ions, especially at relatively high temperatures (>45 °C) or low temperatures (<0 °C) [5–9]. Hence, BMSs are mostly designed

to take temperature as a monitoring index for estimating the states, degradation, and safety of LIBs [10–12].

Capacity loss and internal resistance growth have been considered as the main indices used to illustrate battery degradation [13,14]. The estimation of the state of charge (SOC), state of health (SOH), and state of safety (SOS) has been investigated in recent years [2,15–17]. Taking temperature into consideration, researchers have also proposed related work on the aging mechanism and safety evolution of LIBs at high- or low-temperature conditions [18–21]. Experimental methods and analyses have also been conducted recently to reveal the trends of battery aging or thermal states across a wide temperature range [22,23]. The aging path and degradation characteristics at low temperatures have been analyzed in detail to provide evolution laws [24]. Low-temperature working conditions constantly occur in the winter season, which may limit ability and influence degradation during battery cycling [25]. To suppress the effects of low temperature, heat generation and pre-heating strategies have been proposed [25,26]. Battery cycling also needs to be considered in combination with temperature conditions to illustrate long-term characteristics [27,28]. Charging or discharging with a large current rate (fast charging) at low temperature is also a further research direction for analyzing the dynamic energy supply ability of LIBs, because a large current brings severe polarization and solid electrolyte interphase (SEI) growth to the battery [29–32].

This paper explores the degradation and safety characteristics of LIBs at low temperature. Various temperatures, cycle numbers, charging/discharging rates, and depths of discharge/charge (DODs/DOCs) are taken into consideration to test the battery cycling performance. Based on experimental results, the trends of capacity loss, internal resistance growth, and open-circuit voltage are analyzed. Moreover, thermal runaway (TR) tests were conducted to illustrate the thermal characteristics and safety evolution of LIBs at low temperature. Several evolution rules of degradation and safety have been determined as a reference to support further design of thermal management strategies or lifetime estimation.

2. Battery Experiment System

2.1. Cell Information

This study employed commercial cylindrical 18650 (Sony US18650VTC6 manufactured in Changzhou, China) lithium-ion batteries as test samples to explore their electrochemical performance, cycling behavior, thermal behavior, and safety characteristics under low-temperature conditions. The detailed parameter information is shown in Table 1. To decrease the influence of cell variation, an amount of 18650 LIBs (100 cells) from the same producer and the same single production batch was applied in this study. Before conducting all the designed experiments, we tested the capacity of these fresh cells and selected cells with similar capacity to control the capacity variation within 10 mAh. Therefore, all tested cells could maintain a stable cell-to-cell variation with each other, to ensure the testing consistency and avoid experimental uncertainty as much as possible.

Table 1. The parameter information of the battery cell sample.

Type	Value
positive material type	NCM
rated capacity/voltage	3000 mAh, 3.6 V
max charging voltage	4.20 ± 0.05 V
cutoff voltage	2.50 V
max discharging current	30 A, 60 Ah peak
diameter/height	18 mm/65 mm
weight	45.1 ± 1.5 g

2.2. Experiment Conditions

(1) Battery cycle testing system

The battery cycle testing system consists of four components as follows.

a. a high-precision battery tester (CT-4008-5V12A-DB, NEWARE Technology LLC, Shenzhen, China) with ±0.1% voltage/current accuracy, including master unit and eight channels supporting 5V12A simultaneous charging/discharging, as shown in Figure 1a;

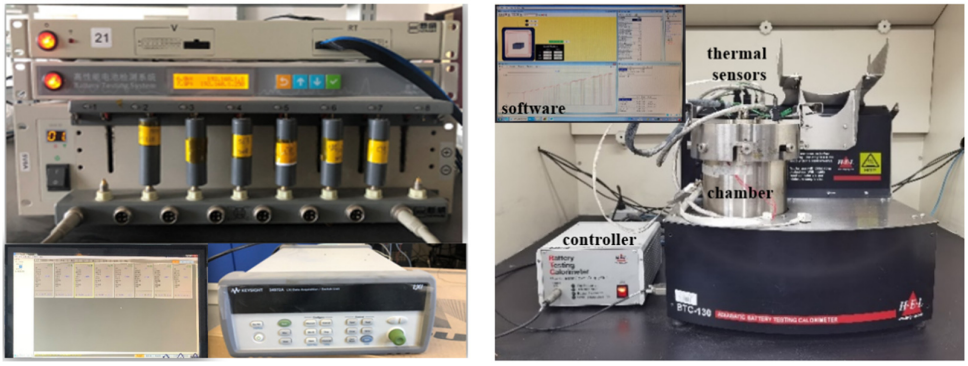

(**a**) (**b**)

Figure 1. Battery performance test system: (**a**) battery cycle tester, (**b**) accelerating rate calorimeter.

b. low-temperature chamber to −40 °C, providing ±2 °C accuracy;
c. data acquisition unit (CA-4008-1U-VT, NEWARE Technology LLC) for battery charging/discharging data collection, providing ±0.1 °C temperature measurement accuracy, and ±0.001 V voltage measurement accuracy;
d. PC and its control software.

(2) Battery safety testing system

Accelerating Rate Calorimeters (ARCs) are widely used to study the thermal characteristics and safety of LIBs. This study employed an HEL BTC-130 ARC with a maximum tracking temperature of 500 °C, a maximum vessel pressure of 4 bar, and high-stability temperature control of 0.1% accuracy. The BTC-130 has a can with a 130 mm outer diameter and 20 mm thickness, and it is controlled by software to construct an adiabatic condition for battery samples by heat compensation, as shown in Figure 1b. The thermal characteristics of LIB samples with varying aging levels under low temperature were investigated to explore the evolution of safety performance.

2.3. Experiment Setups

(1) Battery cycling test

This study conducted a battery accelerated aging test within a low-temperature chamber (−20 °C low temperature). The accelerated aging test employed an aging protocol with constant-current constant-voltage (CC-CV) charging, in which the CC stage held 3 C-rate fast charging until 4.2 V, and the CV stage held until the current dropped to 0.05 C. Battery discharging used constant current at a C-rate of 3 until the battery voltage reached the cutoff voltage 2.5 V. Five groups of LIB samples (six cells in every group) were aged to 0, 15, 25, 50, 75, 100, 125, and 150 cycles for comparative studies on battery aging characteristics, electrical–thermal properties, and battery safety.

(2) Battery charging/discharging test at low temperature

This study implemented the experimental protocol shown in Table 2 to explore the effects of different aging paths at low temperatures on the degradation rate and internal

resistance growth of LIBs. The protocol in Table 2 specifically investigates the influence of charge–discharge rates (0.33 C to 3.00 C) on the aging characteristics of LIBs under low-temperature conditions. All cells were fully charged/discharged during this protocol.

Table 2. Battery charging/discharging test protocol.

Type	Charging Rate (C)	Discharging Rate (C)	Temperature (°C)
1	0.33	3.00	−20
2	0.50	3.00	−20
3	0.66	3.00	−20
4	1.00	3.00	−20
5	1.50	3.00	−20
6	3.00	0.33	−20
7	3.00	0.50	−20
8	3.00	0.66	−20
9	3.00	1.00	−20
10	3.00	1.50	−20

(3) Battery aging test under various temperatures

This study employed the experimental protocol shown in Table 3 to investigate the impact of fast charging–discharging on battery aging characteristics under various temperatures (−20 °C to 25 °C). All cells were fully charged/discharged during this protocol.

Table 3. Battery aging test protocol under various temperatures.

Type	Charging/Discharging Rate (C)	Cycles with HPPC Test	Temperature (°C)
1	3.00/3.00	0, 25, 50, 75, 100, 125, 150	−20
2	3.00/3.00	0, 25, 50, 75, 100, 125, 150	−10
3	3.00/3.00	0, 25, 50, 75, 100, 125, 150	0
4	3.00/3.00	0, 25, 50, 75, 100, 125, 150	25
5	3.00/3.00	0, 25, 50, 75, 100, 125, 150	45

(4) Battery test with various DOD/DOC at low temperature

This study also employed the protocol shown in Table 4 to explore the influence of voltage range during charge–discharge cycles on aging characteristics under various low-temperature conditions.

Table 4. Battery test protocol with various DODs/DOCs at low temperature.

Type	Charging/Discharging Rate (C)	DOD/DOC (V)	Temperature (°C)
1	1.00/1.00	2.50–3.80	−20
2	1.00/1.00	2.50–4.00	−20
3	1.00/1.00	2.50–4.10	−20
4	1.00/1.00	2.50–4.20	−20
5	1.00/1.00	3.00–4.20	−20
6	1.00/1.00	3.20–4.20	−20
7	1.00/1.00	3.40–4.20	−20

(5) Battery thermal runaway test

For the battery thermal runaway test, the Heat–Wait–Search (H-W-S) test was employed to show the thermal characteristics of LIBs. The Heat–Wait–Search (H-W-S) test

is an important adiabatic calorimetry method for constructing adiabatic conditions and determining the key temperatures of exothermic reactions for LIBs. In this study, all the ARC tests (H-W-S tests) had the same setups, that is, the initial temperature was 40 °C, every temperature increment was 5 °C, the maximum temperature to search for was 350 °C, and the calibration time and search time were 30 min and 5 min, respectively. During the H-W-S test, the battery sample underwent calibration from the initial temperature (40 °C) and then entered the search phase for exothermic reactions and the track phase for the thermal process. Once the self-heating rate was ≥0.02 °C/min, the battery cell reached temperature T1 (the start of self-heating); then, when the exothermic rate was ≥1 °C/s, the cell reached temperature T2 (the start of thermal runaway); moreover, the highest temperature was tracked as T3 (the maximum temperature during thermal runaway). Precise temperature measurement of battery self-heating behavior can help illustrate the thermal runaway characteristics of LIBs.

(6) Battery HPPC test

To test the internal resistance of LIBs, the Hybrid Pulse Power Characterization (HPPC) test was employed during battery cycling. Before the HPPC test, battery cells were charged to a fully charged state (100% SOC); then, the pulse protocol shown in Figure 2 was applied to cells every 10% SOC (1 C discharge). The main parameters of the HPPC test are a 10 s discharge with a 1 C current, a 40 s rest duration, and then a 10 s charge with a 0.75 C current, as shown in Figure 2. With the HPPC pulse, the ohmic resistance and polarization resistance during the discharge/charge pulse can be calculated by Equations (1)–(4).

$$R_{o-dch} = \frac{U_1 - U_2}{I_{dch}} \quad (1)$$

$$R_{p-dch} = \frac{U_2 - U_3}{I_{dch}} \quad (2)$$

$$R_{o-ch} = \frac{U_1' - U_2'}{I_{ch}} \quad (3)$$

$$R_{p-ch} = \frac{U_3' - U_2'}{I_{ch}} \quad (4)$$

where I_{dch} is the discharge current (1 C), R_{o-dch} is the ohmic resistance of the discharge pulse, R_{p-dch} is the polarization resistance of the discharge pulse, I_{ch} is the charge current (0.75 C), R_{o-ch} is the ohmic resistance of the charge pulse, and R_{p-ch} is the polarization resistance of the charge pulse.

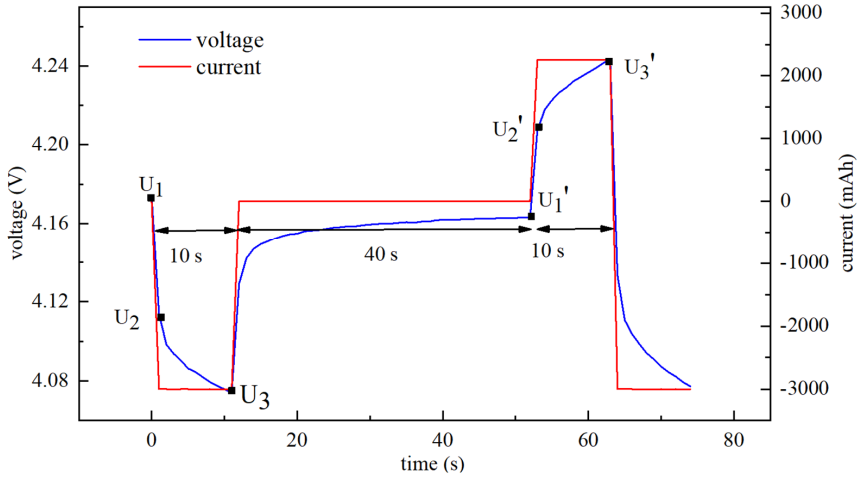

Figure 2. Hybrid Pulse Power Characterization (HPPC) test protocol.

3. Experimental Results and Analysis

3.1. Electrical Parameter Trends for Aged Battery at Low Temperature

3.1.1. Open-Circuit Voltage

Figure 3 shows the open-circuit voltage (OCV) curves of aged batteries at different ambient temperatures, showing significant temperature sensitivity to OCV. Since OCV is positively related to SOC, all OCV values across 0–100% SOC remain in the range of 2.95 V–4.17 V when the ambient temperature is between 0 °C and 45 °C. When the temperature is below 0 °C, the OCV at low SOC increases markedly. For example, the OCV at −10 °C and 0% SOC is larger than 3.2 V, while the OCV at −20 °C and 0% SOC can be even larger than 3.6 V for an aged battery (125 cycles and 150 cycles). This indicates a flatter OCV-SOC relationship at low temperatures, especially for low SOC values (such as SOC < 50%).

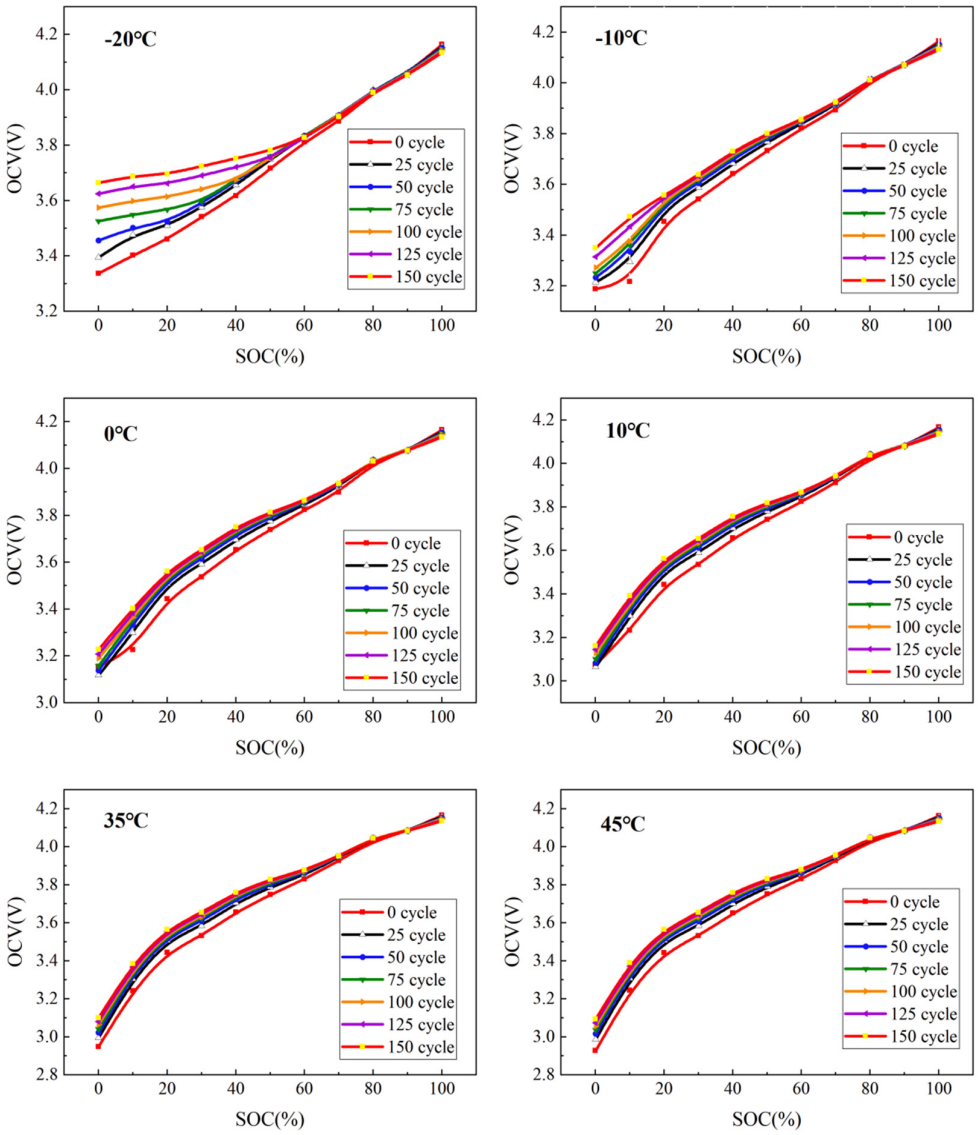

Figure 3. Open-circuit voltage of aging battery at different ambient temperatures.

Figure 3 also demonstrates the influence of battery degradation on OCV under low temperature. OCV under different aging degrees exhibits nearly identical trends at a certain temperature. Within the low SOC range (0% to 60%), OCV progressively rises with aging severity, while OCV exhibits almost a slight change within 60% to 100% SOC. Moreover, increased battery aging flattens OCV's relationship with SOC. For example, at −20 °C and

0% SOC, the fresh cell has an OCV of 3.34 V, while the 150-cycle-aged cell reaches an OCV of 3.66 V, which is a 0.32 V increase in OCV.

3.1.2. Internal Resistance

Internal resistance can cause irreversible heat during the electrochemical reactions of LIBs, which then reduces battery charging/discharging efficiency. Using the HPPC method, the internal resistance of aged batteries was measured at low temperatures, as shown in Figure 4. The resistance variations in Figure 4 were measured for a battery discharged from 20 to 80% SOC (common working range without severe polarization reactions) under different temperatures (−20 °C to 45 °C). The total internal resistance is divided into ohmic and polarization resistance, as shown in Figure 4a,b. Internal resistance holds strong temperature dependence, and it increases with decreasing temperature, particularly at low temperatures. At −20 °C, fresh batteries have ohmic, polarization, and total resistances of 109.0 mΩ, 44.2 mΩ, and 153.3 mΩ, respectively, which are 5.6, 3.3, and 4.7 times higher than those at 25 °C. This also demonstrates that ohmic resistance is more sensitive to temperature than polarization resistance. The resistance variations may be caused by reduced ionic conductivity and lower battery electrochemical activity at low temperature.

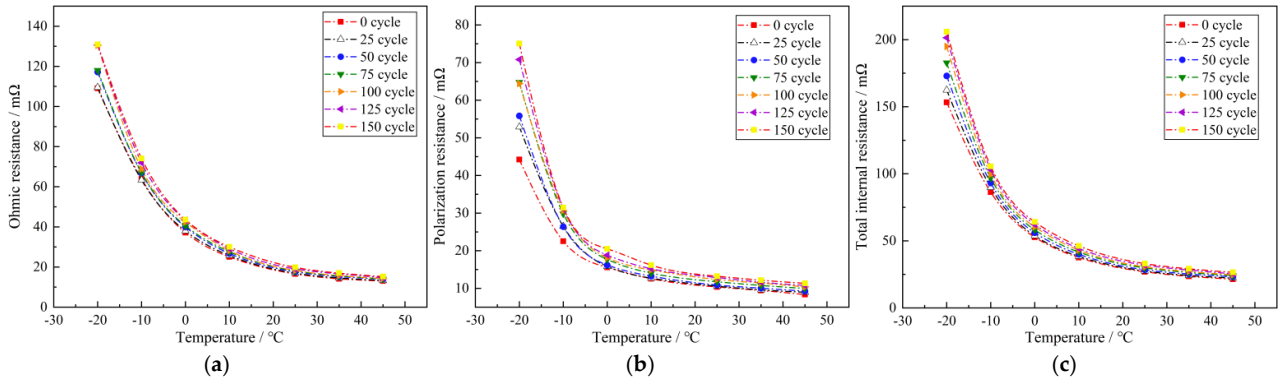

Figure 4. Internal resistance of aging battery at different ambient temperatures: (**a**) ohmic resistance, (**b**) polarization resistance, (**c**) total internal resistance.

Polarization resistance in aged batteries exhibits greater temperature sensitivity, increasing with aging severity. For example, the polarization resistance of the 150-cycle-aged battery at −20 °C reaches 5.7 times its value at 25 °C. Higher aging degrees reduce the ohmic resistance proportion within total resistance. From the temperature aspect, lower temperatures increase the fraction of ohmic resistance between −10 °C and 45 °C; however, excessive polarization resistance significantly raises its fraction and reduces the ohmic proportion at −20 °C, which shows that the battery polarization may dramatically increase once the temperature is lower than a certain value.

3.2. Influence of Low Temperature on Battery Degradation Characteristics

3.2.1. Capacity Trends at Various Temperatures

The electrolyte conductivity and lithium-ion diffusion in porous electrodes are significantly reduced at low temperatures. To investigate the capacity trends, LIBs underwent 150 aging cycles at five different temperatures (−20 °C, −10 °C, 0 °C, 10 °C, and 25 °C). The capacity test and HPPC tests were conducted every 25 cycles. Figure 5a,b depict the charging and discharging capacity evolution during the first 1–25 cycles at the five temperatures. The results shown in Figure 5 are relative percentages of capacity, and the baseline is the charge capacity and discharge capacity at the second cycle of the cell; thus, the results may start at greater than 100% at the beginning of Figure 5a. Before the first cycle of this aging experiment, the battery samples were discharged with 0.3 C current to 2.5 V at 25 °C

and then put under low-temperature conditions. Due to severe polarization under low-temperature conditions, the initial charge/discharge capacity of LIBs at the first cycle tends to be abnormally high. Therefore, the second-cycle capacity was used as the baseline. It is obvious that battery degradation is accelerated at low temperature. In particular, the discharge/charge capacities dropped from an initial 2716.1 mAh/2696.2 mAh (the charge and discharge capacity at the second cycle) to 88.2%/87.0% retention at −20 °C temperature, whereas at 25 °C temperature, battery capacity decreased from 2923.1 mAh/2917.9 mAh to 95.2%/95.1% retention at the same 1–25 cycles.

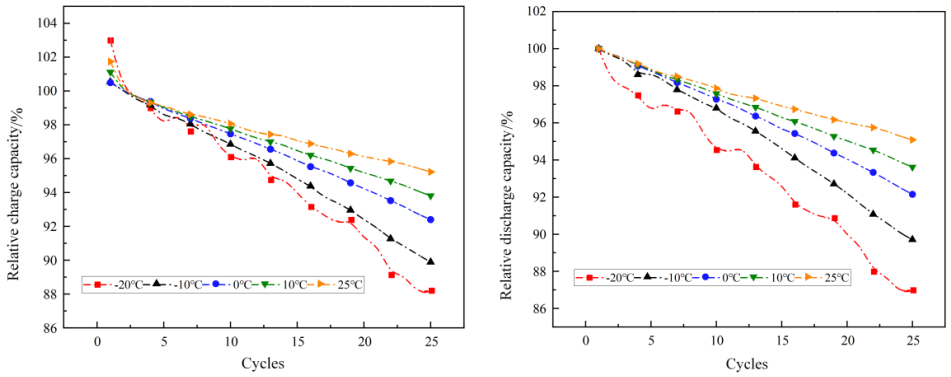

(**a**) (**b**)

Figure 5. Relative percentage of charge/discharge capacity at different ambient temperatures during the first 1–25 cycles: (**a**) charging capacity, (**b**) discharging capacity.

For the considered 3 C-rate discharge process, we obtained the capacity–voltage variations during 1, 25, and 150 discharge cycles at different temperatures, as shown in Figure 6. Due to the low temperature, LIBs exhibit severe polarization and large initial voltage drops in the low SOC range. The polarization resistance dramatically increases, and high-rate discharge generates internal heat, resulting in more consumption of battery energy and less available capacity.

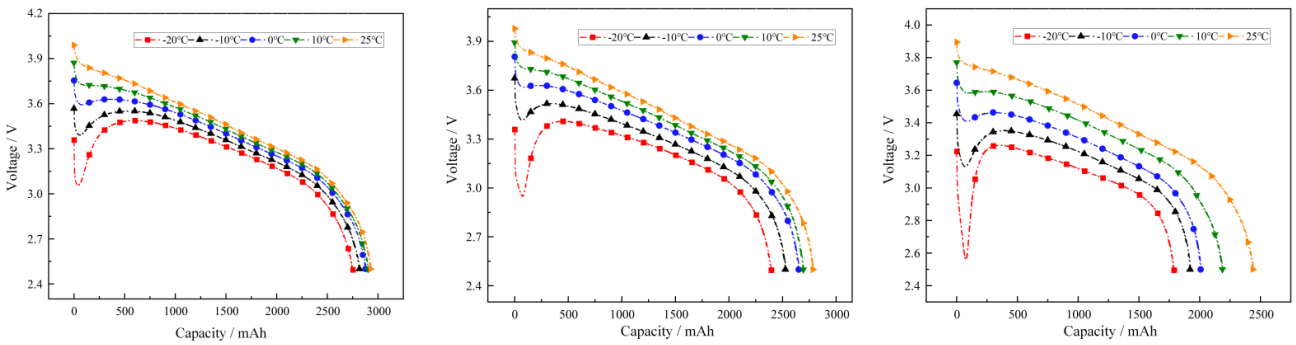

(**a**) (**b**) (**c**)

Figure 6. Capacity–voltage variations during 1, 25, and 150 discharge cycles at different temperatures: (**a**) the 1st cycle, (**b**) the 25th cycle, (**c**) the 150th cycle.

From Figure 6, with battery degradation increasing, the initial voltage drop at low temperature is more obvious. At the lowest temperature (−20 °C), the initial discharge voltage declines from 3.06 V (cycle 1) to 2.95 V (cycle 25) and 2.56 V (cycle 150), representing a 500 mV reduction after 150 cycles. This phenomenon implies that the battery will confront operational failure if the initial voltage drops below 2.50 V during this 3 C-rate cycling. At the same time, the maximum voltage rebound also decreases from 3.59 V to

3.26 V after 150 cycles, confirming that the aged battery is no longer suitable for high-rate discharging/charging at this low temperature.

During low-temperature charging, lithium-ion diffusion in graphite anodes is suppressed, and increased electrolyte viscosity reduces intercalation rates, causing lithium plating and accelerating capacity degradation. The relative discharge capacity loss at different temperatures is calculated every 25 aging cycles and shown in Figure 7. The baseline is the rated capacity of a fresh battery in a 25 °C/0.3 C discharge test. It can be noted that after 150 cycles, lower temperatures accelerate degradation, with 83.3% capacity retained at 25 °C versus 74.2% retained at −20 °C.

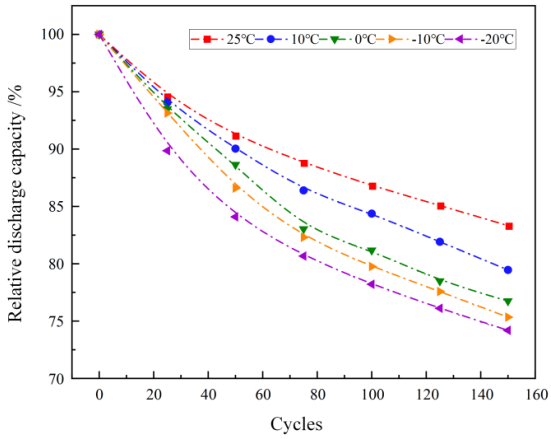

Figure 7. The relative percentage of discharge capacity at different temperatures during 0–150 cycles.

3.2.2. Internal Resistance Trends at Various Temperatures

This section analyzes the increase rate of internal resistance at different temperatures (−20 °C to 25 °C), as shown in Figure 8. The baseline is the internal resistance of a fresh battery. The internal resistance is calculated for the 20–80% SOC operational range every 25 cycles and divided into ohmic, polarization, and total internal resistance. For ohmic resistance, when the ambient temperature is above 0 °C, lower temperatures affect the increase in ohmic resistance substantially, with ohmic resistance rising by 15.4% after 150 cycles at 25 °C and 19.7% at 0 °C. This may be caused by lithium plating at 0 °C, where deposited reaction products thicken the solid electrolyte interphase (SEI). When the temperature is below 0 °C, ohmic resistance growth is only 12.4% after 150 cycles at −20 °C, seeming to slow down. This may be attributable to electrolyte ionic conductivity enhanced by the generated heat of excessive polarization resistance.

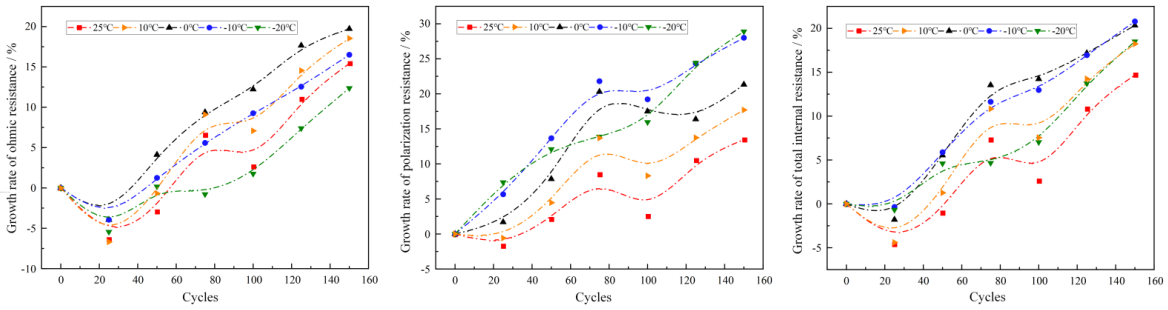

Figure 8. Increase rate of internal resistance at different temperatures during 0–150 cycles: (**a**) ohmic resistance, (**b**) polarization resistance, (**c**) total internal resistance.

As shown in Figure 8b, polarization resistance grows by 28.9% at −20 °C and 13.5% at 25 °C after 150 cycles, which indicates exacerbated polarization of aged batteries under

low-temperature conditions. For the increase rate of internal resistance from −20 °C to 25 °C, the maximal point of total resistance growth occurs at −10 °C, reaching 20.8% after 150 cycles. This phenomenon proves that a shift may occur due to the slowed ohmic resistance growth between −10 °C and 0 °C.

3.3. Influence of Charge/Discharge Rate on Battery Degradation Characteristics

3.3.1. Capacity Trends at Various Rates

This section provides the capacity trends at various rates, as shown in Figure 9. Significant capacity instability can be achieved by severe polarization during fast charging–discharging under low-temperature conditions. The relative capacity changes at the first 1–25 cycles under various charging and discharging rates are presented in Figures 9a and 8b, respectively.

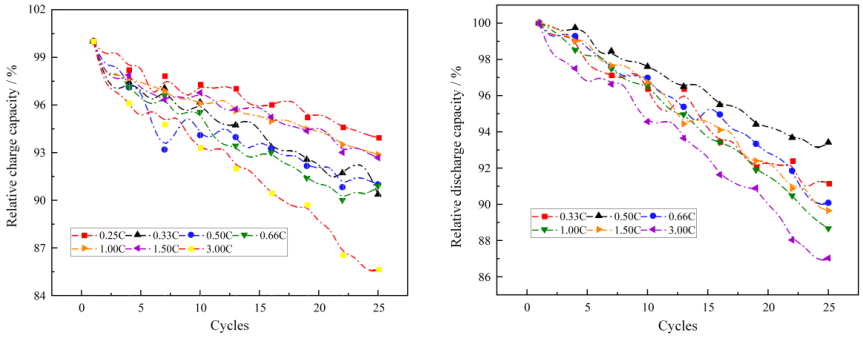

(**a**) (**b**)

Figure 9. Relative percentage of charge/discharge capacity at different charging/discharging rates during the first 1–25 cycles: (**a**) charging capacity, (**b**) discharging capacity.

As shown in Figure 9, during 3 C-rate charging–discharging at −20 °C, the LIB cell is charged only 2396.9 mAh after 25 aging cycles, which is 85.7% of the initial capacity. For discharge rates between 0.33 C and 0.50 C, higher rates slow the capacity degradation, which is attributable to the internal heat generated by enhanced electrochemical activity. Conversely, discharge rates exceeding 0.50 C accelerate capacity degradation. During 3 C-rate discharging at -20 °C, the LIB cell is charged merely 2389.3 mAh (87.0% retention) after 25 cycles.

Figure 10a–c also present the capacity–voltage evolution during the 1st, 25th, and 150th charging cycles under different rates at −20 °C. Higher charging rates elevate voltage plateaus and intensify polarization, resulting in accelerated capacity degradation, which means less capacity at 3 C-rate charging than that at 1.50 C after 25 cycles. This disparity widens during battery cycling, where 3 C-rate charging yields only 2396.9 mAh capacity for the LIB after the 150th cycle.

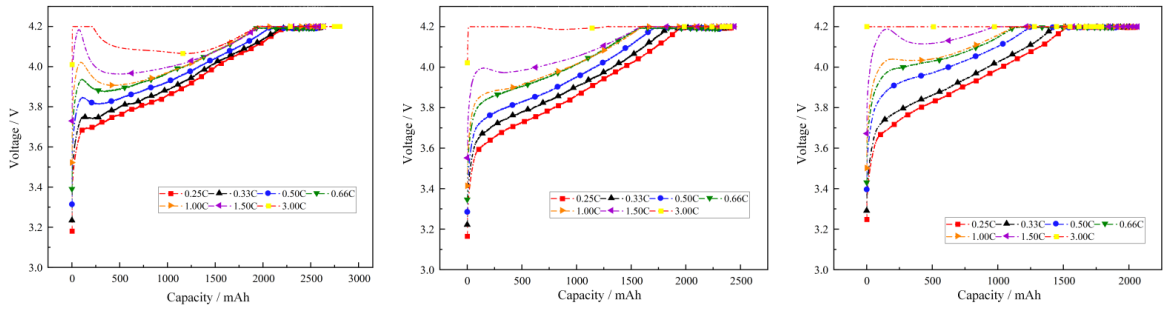

(**a**) (**b**) (**c**)

Figure 10. Capacity–voltage variations during 1, 25, and 150 discharge cycles at different charging/discharging rates: (**a**) the 1st cycle, (**b**) the 25th cycle, (**c**) the 150th cycle.

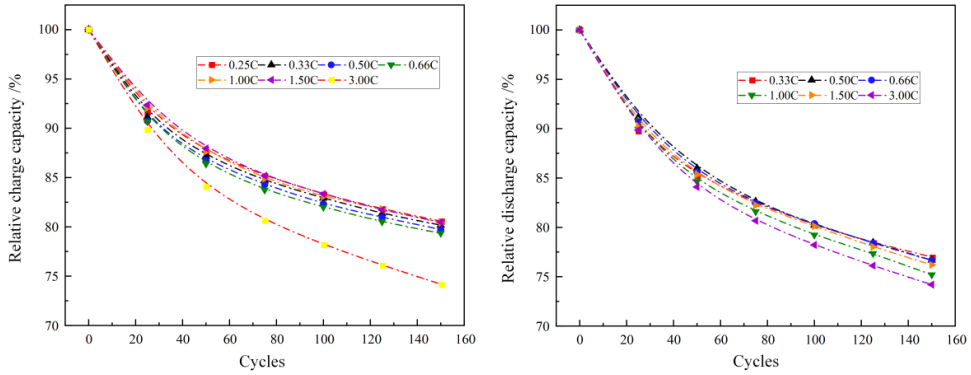

(**a**) (**b**)

Figure 11. The relative percentage of cell capacity at different charging/discharging rates during 0–150 cycles: (**a**) charge capacity, (**b**) discharge capacity.

As shown in Figure 11, the capacity retention drops to 80.6% after 150 aging cycles at −20 °C with 0.25 C charging and 3 C-rate discharging. However, with small charging currents, the battery still exhibits a rapid capacity degradation, which demonstrates the effect of low-temperature conditions. It is worth noting that higher rates slow capacity degradation between discharge rates of 0.33 C and 1.00 C. Specifically, the battery capacity at 0.33 C–0.66 C discharges shows similar degradation, stabilizing around 76.6% retention after 150 cycles. When the discharge rate reaches 1.50 C, increased heat generation enhances electrochemical activity, yielding 76.2% retention, which is a lower capacity loss than that at 1 C. However, 3 C-rate discharging causes severe polarization and performance deterioration, which then accelerates capacity degradation.

3.3.2. Internal Resistance Trends at Various Rates

Internal resistance is also significantly impacted by cycling rates at various low-temperature conditions. The relative resistance changes across charging rates (0.25 C–3.00 C) with fixed 3.00 C discharge at −20 °C are calculated every 25 cycles and presented in Figure 12a–c. Between 0.25 C and 0.66 C charging, polarization resistance growth accelerates with increasing rates, reaching 9.1% at 0.25 C and 15.4% at 0.66 C after 150 cycles. Due to severe polarization in aged batteries, polarization resistance growth rates are twice as large as the rates of ohmic resistance in this range. Total resistance growth similarly increases with higher charging rates in the 0.25 C–0.50 C range, reaching 6.0% at 0.25 C and 9.1% at 0.50 C after 150 cycles. Then, at 1.00 C–1.50 C, total resistance growth stabilizes near 9.1%.

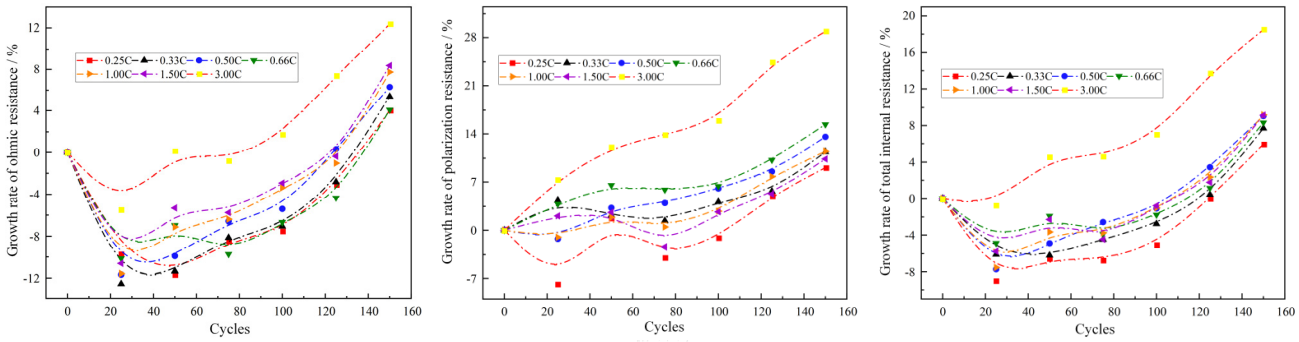

(**a**) (**b**) (**c**)

Figure 12. Increase rate of internal resistance at different charging/discharging rates during 0–150 cycles: (**a**) ohmic resistance, (**b**) polarization resistance, (**c**) total internal resistance.

3.4. Influence of DOD/DOC on Battery Degradation Characteristics

3.4.1. Capacity Trends at Various DODs/DOCs

Voltage charging/discharging windows significantly impact lithium-ion battery performance and cycle life. This section presents the influence of both the depth of discharge (DOD) and depth of charge (DOC) on battery degradation under low-temperature conditions.

Figure 13a–c depict capacity–voltage evolution during the 2nd, 25th, and 150th charging cycles under different charging/discharging cutoff voltages (DODs/DOCs). Higher cutoff voltages increase both constant-current phase capacity and total charging capacity. The constant-current phase is usually shortened with higher polarization, especially under −20 °C conditions, as shown in Figure 13. Due to severe polarization at low temperature, batteries cycle between 2.5 V and 3.8 V and operate almost in constant-voltage mode, causing an immediate voltage surge to the cutoff voltage value. However, when the cutoff voltage $\geq$ 4.0 V, a higher constant-current capacity can be achieved, because internal self-heat generation of LIBs is enough to partially mitigate polarization, and then the constant-current phase is extended, as shown in Figure 13. Initial capacities at cycle 2 are measured as 1096.8 mAh (3.80 V), 1726.5 mAh (4.00 V), 2027.4 mAh (4.10 V), and 2365.4 mAh (4.20 V). After 150 cycles, battery capacities reduce to 1073.9 mAh, 1624.9 mAh, 1753.4 mAh, and 1950.6 mAh, representing 2.1%, 5.9%, 13.5%, and 17.5% reductions, respectively.

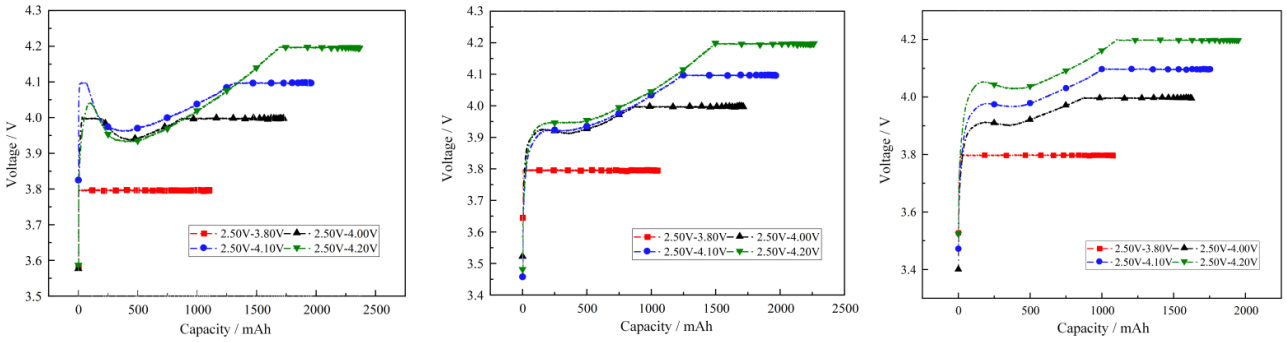

Figure 13. Capacity–voltage variations during 2, 25, and 150 discharge cycles at different DODs/DOCs: (**a**) the 2nd cycle, (**b**) the 25th cycle, (**c**) the 150th cycle.

At −20 °C with 3.00 C charging, severe polarization restricts operation within given voltage limits, while initial voltage drops rapidly due to polarization during 3.00 C discharging. This abrupt voltage sag to cutoff levels prevents complete discharge under low-temperature conditions.

Figure 14 presents the relative capacity retention across different voltage cutoffs (DODs/DOCs), which is calculated every 25 aging cycles, and the baseline is the capacity of a fresh battery at 25 °C/0.3 C discharge condition. Increasing aging severity progressively reduces discharge capacity. Higher charge cutoff voltages accelerate degradation; similarly, lower discharge cutoff voltages intensify capacity degradation.

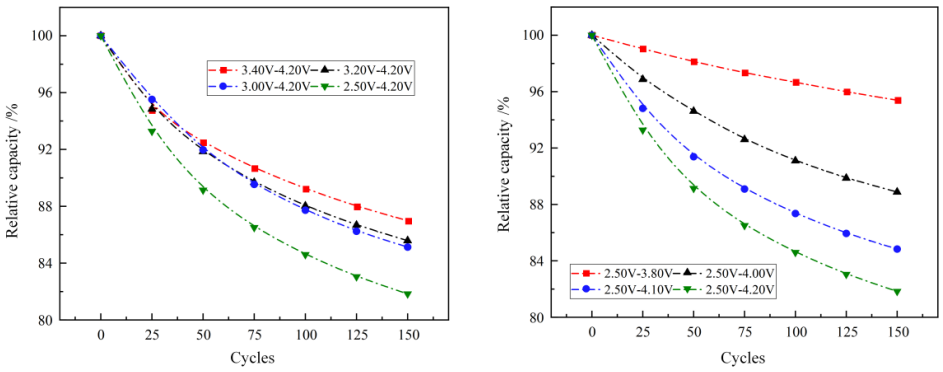

(**a**) (**b**)

Figure 14. The relative capacity percentage at different DODs/DOCs during 0–150 cycles: (**a**) DOD, (**b**) DOC.

3.4.2. Internal Resistance Trends at Various DODs/DOCs

At −20 °C and 1.00 C cycling, the relative internal resistance changes under various discharge cutoffs (2.50 V, 3.00 V, 3.20 V, 3.40 V) and a fixed 4.20 V charge cutoff is calculated every 25 cycles and presented in Figure 15. The baseline is the internal resistance of fresh batteries. The relative change in ohmic resistance reaches its minimum after 25 cycles. Relative to this minimum, ohmic resistance increases by 10.3% (2.50 V), 8.2% (3.00 V), 6.5% (3.20 V), and 3.5% (3.40 V) after 150 cycles, which shows that a larger DOD accelerates ohmic resistance growth.

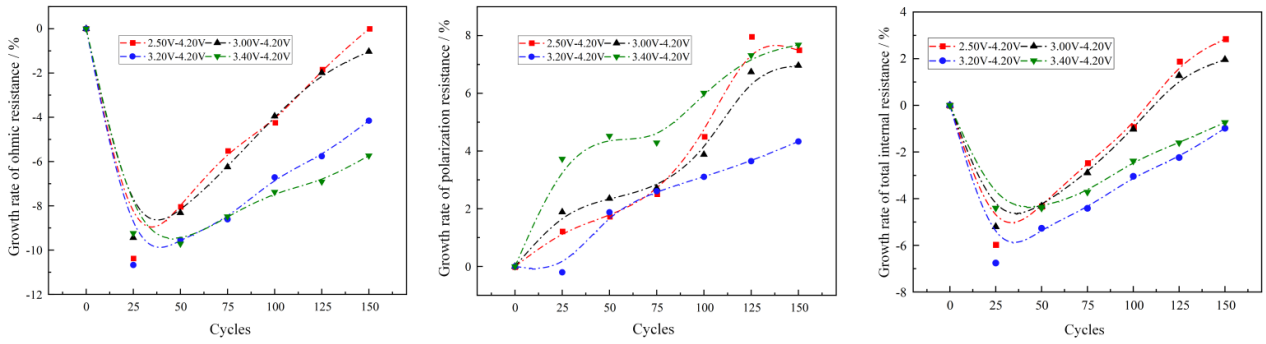

(**a**) (**b**) (**c**)

Figure 15. Increase rate of internal resistance at different DODs during 0–150 cycles: (**a**) ohmic resistance, (**b**) polarization resistance, (**c**) total internal resistance.

From the cycling process shown in Figure 15, it can be seen that polarization resistance growth increases progressively with lower discharge cutoffs (2.50 V: 7.5%, 3.00 V: 7.0%, 3.20 V: 4.3% after 150 cycles), which demonstrates that a larger DOD accelerates polarization resistance growth. However, batteries cycled between 3.40 V and 4.20 V exhibit 7.7% polarization resistance growth, which may be due to the severe polarization within this narrow voltage window and insufficient relaxation time for depolarization.

The DOD and DOC may cause different cycling paths and heat-induced electrochemical activation of LIBs. On one hand, a smaller DOD shortens cycling time, reducing polarization and particle surface stress inside LIBs. Then, partial lithium-ion intercalation during this shallow cycling (small DOD) minimizes the loss of active lithium ions for the battery. On the other hand, due to elevated polarization resistance at low temperature, large discharge currents during deep discharge (large DOD) generate substantial inner heat, which enhances electrolyte conductivity and electrochemical activity.

3.5. Thermal Runaway Results at Different Aging Cycles

This section provides the thermal evolution of the battery after degradation at low temperature. Thermal runaway tests were conducted for cells under different aging cycles, that is, fresh, 15th, 25th, 75th, and 150th cycles. All cells were charged to a fully charged state (100% SOC) before the thermal runaway tests were conducted. Figure 16a–e display thermal runaway curves for fully charged battery samples at 0, 15, 25, 75, and 150 aging cycles. All samples exhibited catastrophic damage with complete destruction of cathode venting structures. Violent ejection of cell materials and explosions occurred during testing, accompanied by significant toxic gas release. Abundant charred black powder residue was dispersed throughout the calorimeter vessel.

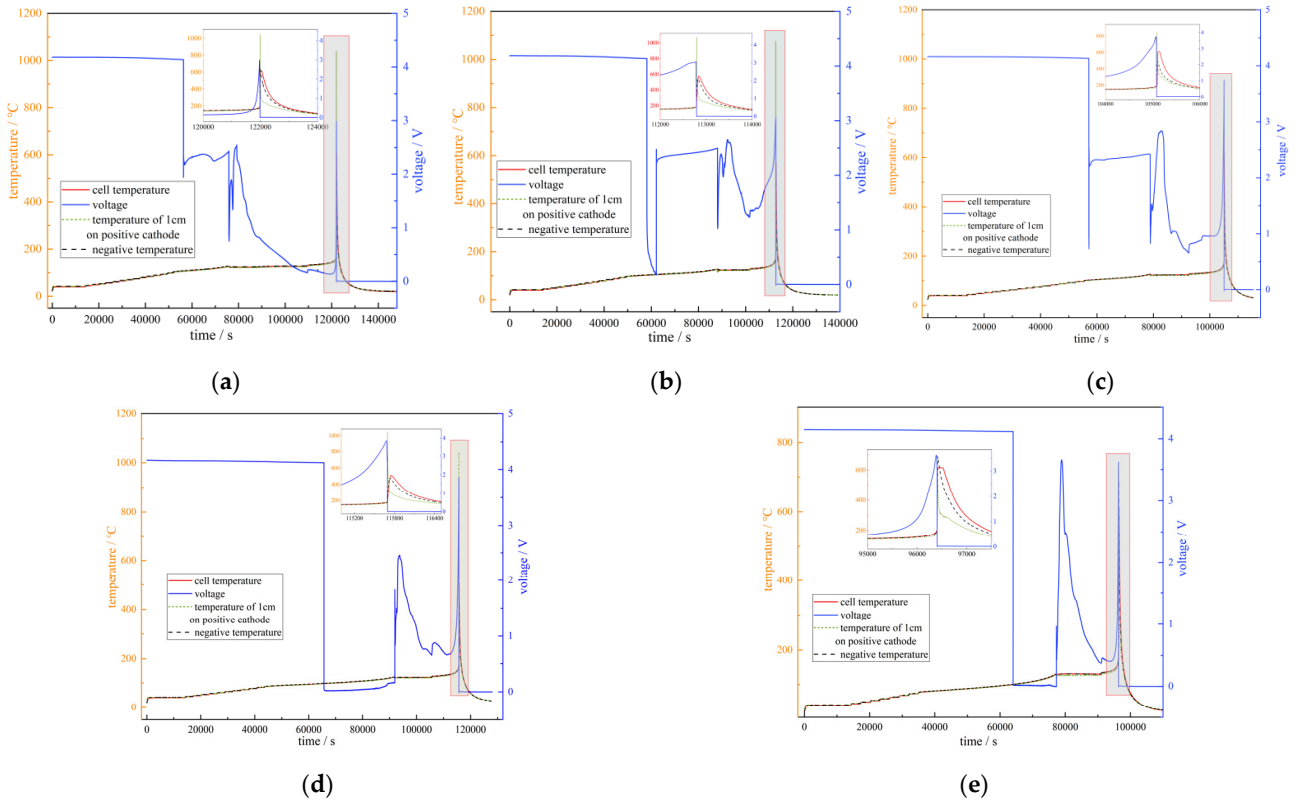

Figure 16. Thermal runaway curves for fully charged battery samples at (**a**) 0, (**b**) 15, (**c**) 25, (**d**) 75, and (**e**) 150 aging cycles.

As shown in Figure 16, with battery aging at low temperature, the thermal activation also fades; an example is the peak temperature (T3) during thermal runaway. To compare the thermal runaway characteristics more clearly, the performance indices, such as temperature range, voltage range, T1 (the temperature of the start of battery self-heating), T2 (the start point of thermal runaway), T3 (the highest temperature during thermal runaway), and the maximum self-heating rate, are presented in Table 5. As shown in Table 5, the thermal runaway behavior of the battery with different aging cycles does not follow linear trends, and a fully charged battery at 150 aging cycles still holds similar energy, reaching a high T3 value and self-heating rate during thermal runaway. Moreover, the thermal characteristics of fully charged cells with different aging cycles depend on the value of T2; that is, a larger T2 causes a larger T3 and self-heating rate, which may demonstrate heavy thermal runaway of this cell. This may be due to greater self-heat generated in the period between T1 and T2, which is the self-heat accumulation period before thermal runway.

Table 5. The performance indices of temperature and voltage during thermal runaway experiments.

Cycle	Temperature Range (°C)	Voltage Range (V)	T1 (°C)	T2 (°C)	T3 (°C)	dT/dt (°C/s)
Fresh	22.527–612.996	0–4.186	156.231	200.349	612.996	346.567
15th	20.869–575.049	0–4.191	177.165	197.717	575.049	251.835
25th	23.798–613.497	0–4.164	156.960	204.618	613.497	350.021
75th	19.278–507.990	0–4.165	169.769	188.253	507.990	192.052
150th	20.537–614.225	0–4.149	173.278	208.643	614.225	349.147

3.6. Discussion

3.6.1. Capacity Characteristics at Low Temperature

(a) Lower temperatures accelerate capacity degradation and amplify initial voltage transients of LIBs during the charge/discharge process. At −20 °C, severe capacity instability occurs, and an additional 10% capacity degradation happens compared to capacity degradation at 25 °C. Charging polarization forces premature constant-voltage mode initiation, and then subsequent heat generation later restores constant-current charging.

(b) At low temperature, higher charge rates elevate voltage plateaus and polarization severity, accelerating the capacity degradation of LIBs. However, the capacity degradation is not linearly related to the charge rate or discharge rate. Experimental results show that charging at a C-rate of 1–1.5 reduces degradation rates of LIBs due to beneficial internal heating, which improves electrochemical activity inside the battery. Higher discharge rates increase voltage rebound amplitude. Progressive aging further amplifies this rebound and discharge polarization. Battery capacity degradation only holds linear trends under a 0.66 C charge rate. This means that an extreme point can be optimized with the charge rate or discharge rate for charging protocol design.

(c) Large DOCs and DODs accelerate the capacity degradation of LIBs, and this trend is linear. Moreover, a larger charging cutoff voltage (DOC) has a heavier influence on the capacity degradation than the discharging cutoff voltage (DOD). Narrow voltage windows under low-temperature conditions exacerbate capacity loss due to polarization. Discharge cutoff voltages exert particularly pronounced effects on the capacity retention of LIBs.

3.6.2. Internal Resistance Growth and Characteristics at Low Temperature

(a) Due to plated lithium reacting with the electrolyte, low ambient temperatures significantly increase the ohmic resistance (12.4% increase at −20 °C) to form thicker SEI films. Polarization resistance rises markedly (28.9% increase at −20 °C) due to increased electrolyte viscosity, which impedes lithium-ion transport. The polarization resistance holds a linear relationship with temperature, whereas the ohmic resistance does not have a similarly linear trend. Hence, an extreme point of total resistance (ohmic resistance + polarization resistance) exists at nearly −10 °C.

(b) At low temperature, high charge rates generally increase ohmic and polarization resistance. At 0.66 C, ohmic resistance growth slows due to enhanced heat generation. Charge rates impact resistance growth more substantially than discharge rates. Experimental results show that a 15.4% increase in resistance occurs with a higher charge rate (0.66 C), while a 9.1% increase in resistance happens with a higher discharge rate (1–1.5 C).

(c) At low temperature, large DODs and DOCs progressively increase internal resistance with different cycling durations and heat-induced electrochemical activation. Shallow DODs and DOCs reduce polarization and particle stress through shorter durations and partial lithium-ion intercalation. Ohmic resistance increases by about 7% when the cutoff voltage changes from 3.4 V to 2.5 V, while polarization resistance increases by about 3% when the cutoff voltage changes from 3.4 V to 2.5 V. This may demonstrate that ohmic resistance is more sensitive to low temperature than polarization resistance.

4. Conclusions

For the degradation evolution and safety characteristics of LIBs at low temperature, this paper provides the experimental results and analysis of a 18650 cell with different working conditions. Various temperatures (especially low temperatures), cycle numbers, charging/discharging rates, and depths of discharge/charge (DOD/DOC) are taken into consideration to demonstrate aging trends and thermal characteristics of LIBs under these working conditions. Capacity loss and internal resistance growth (including ohmic and polarization resistance) are selected as degradation indices for LIBs to explore the aging laws. Thermal runaway experiments were also conducted for further safety analysis. Based on these experimental results and law analysis, the inner mechanisms of LIBs, such as plated lithium reacting with electrolyte, heat generation at low ambient temperatures, and so on, have also been provided. Several discussions and tips are presented as a reference for further research on lifetime and safety management strategies for BMSs. Experimental results are mainly analyzed in this study; however, simulations with various indices under low temperature for different types of LIBs can be further investigated. Moreover, inner electrochemical reactions and degradation mechanisms can be analyzed at low temperature. More mechanism and material analyses such as SEM and XPS can be added in future work, and thermal monitoring analysis of cell surface temperature may also be conducted to further support internal heating effects.

Author Contributions: Conceptualization, methodology, validation, formal analysis, investigation, R.W. and B.X.; resources, data curation, B.X.; writing—original draft preparation, R.W.; writing—review and editing, supervision, B.X. All authors have read and agreed to the published version of the manuscript.

Funding: This research received no external funding.

Data Availability Statement: The raw data supporting the conclusions of this article will be made available by the authors on request.

Conflicts of Interest: The authors declare no conflicts of interest.

References

1. Alawi, A.; Saeed, A.; Sharqawy, M.H.; Al Janaideh, M. A comprehensive review of thermal management challenges and safety considerations in lithium-ion batteries for electric vehicles. *Batteries* **2025**, *11*, 275. [CrossRef]
2. Zhang, G.; Wei, X.; Wang, X.; Chen, S.; Zhu, J.; Dai, H. Evolution mechanism and non-destructive assessment of thermal safety for lithium-ion batteries during the whole lifecycle. *Nano Energy* **2024**, *126*, 109621. [CrossRef]
3. Qian, G.; Zheng, Y.; Li, X.; Sun, Y.; Han, X.; Ouyang, M. State of health estimation for lithium-ion batteries using impedance-based simplified timescale information. *Appl. Energy* **2025**, *382*, 125272. [CrossRef]
4. Liu, S.; Nie, Y.; Tang, A.; Li, J.; Yu, Q.; Wang, C. Online health prognosis for lithium-ion batteries under dynamic discharge conditions over wide temperature range. *eTransportation* **2023**, *18*, 100296. [CrossRef]
5. Qu, Y.; Xing, B.; Xia, Y.; Zhou, Q. How does room temperature cycling ageing affect lithium-ion battery behaviors under extreme indentation? *etransportation* **2024**, *20*, 100331. [CrossRef]
6. Park, S.J.; Song, Y.W.; Kang, B.; Kang, M.J.; Kim, M.Y.; Choi, Y.J.; Hong, Y. Effect of High-temperature thermal management on degradation of li-ion battery for fast charging. *IEEE Trans. Transp. Electrif.* **2023**, *10*, 2912–2922. [CrossRef]
7. Ying, P.; Wang, C.; Xia, Y. Role of the temperature and aging in mechanical modeling of the active coating in Li-ion battery. *eTransportation* **2023**, *18*, 100273. [CrossRef]
8. Guo, J.; Ping, P.; Ren, J.; Ren, X.; Gao, W.; Kong, D.; Feng, Z. High-temperature calendar aging at low state-of-charge: Electrochemical degradation, thermal safety implications, and optimal SOC ranges for lithium-ion battery storage and transport. *J. Energy Storage* **2025**, *125*, 116988. [CrossRef]
9. Ma, W.; Yang, X.; Tao, X.; Xie, S. The effect of low-temperature starting on the thermal safety of lithium-ion batteries. *Energy* **2024**, *311*, 133427. [CrossRef]
10. Zhang, G.; Wei, X.; Chen, S.; Han, G.; Zhu, J.; Dai, H. Investigation the degradation mechanisms of lithium-ion batteries under low-temperature high-rate cycling. *ACS Appl. Energy Mater.* **2022**, *5*, 6462–6471. [CrossRef]

11. Velumani, D.; Bansal, A. Thermal behavior of lithium-and sodium-ion batteries: A review on heat generation, battery degradation, thermal runway–perspective and future directions. *Energy Fuels* **2022**, *36*, 14000–14029. [CrossRef]
12. Zhang, G.; Wei, X.; Wang, X.; Zhu, J.; Chen, S.; Wei, G.; Dai, H. Lithium-ion battery sudden death: Safety degradation and failure mechanism. *eTransportation* **2024**, *20*, 100333. [CrossRef]
13. Liu, J.; Zhou, L.; Zhang, Y.; Wang, J.; Wang, Z. Aging behavior and mechanisms of lithium-ion battery under multi-aging path. *J. Clean. Prod.* **2023**, *423*, 138678. [CrossRef]
14. Kim, S.; Jung, H.; Lee, M.; Choi, Y.Y.; Choi, J.I. Model-free reconstruction of capacity degradation trajectory of lithium-ion batteries using early cycle data. *eTransportation* **2023**, *17*, 100243. [CrossRef]
15. Qian, L.; Yi, Y.; Zhang, W.; Fu, C.; Xia, C.; Ma, T. Revealing the Impact of High Current Overcharge/Overdischarge on the Thermal Safety of Degraded Li-Ion Batteries. *Int. J. Energy Res.* **2023**, *2023*, 8571535.
16. Shi, J.; Rivera, A.; Wu, D. Battery health management using physics-informed machine learning: Online degradation modeling and remaining useful life prediction. *Mech. Syst. Signal Process.* **2022**, *179*, 109347. [CrossRef]
17. Wang, Z.; Zhao, Q.; Wang, S.; Song, Y.; Shi, B.; He, J. Aging and post-aging thermal safety of lithium-ion batteries under complex operating conditions: A comprehensive review. *J. Power Sources* **2024**, *623*, 235453. [CrossRef]
18. Shen, W.; Wang, N.; Zhang, J.; Wang, F.; Zhang, G. Heat generation and degradation mechanism of lithium-ion batteries during high-temperature aging. *ACS Omega* **2022**, *7*, 44733–44742. [CrossRef] [PubMed]
19. Zhang, G.; Wei, X.; Chen, S.; Wei, G.; Zhu, J.; Wang, X.; Dai, H. Research on the impact of high-temperature aging on the thermal safety of lithium-ion batteries. *J. Energy Chem.* **2023**, *87*, 378–389. [CrossRef]
20. Gao, X.; Li, K.; Cao, Y.C.; Offer, G.J.; Wang, H. Simulation and understanding of degraded lithium-ion battery self-heating ignition. *Appl. Energy* **2025**, *384*, 125435.
21. Zhang, G.; Shen, W.; Wei, X. Lithium-ion battery thermal safety evolution during high-temperature nonlinear aging. *Fuel* **2024**, *362*, 130845. [CrossRef]
22. Sabeel, K.; Al-Greer, M.; Bashir, I. Advancements in Vibration Testing: Effects on Thermal Performance and Degradation of Modern Batteries. *Batteries* **2025**, *11*, 82. [CrossRef]
23. Hong, H.; Zhu, Y.; d'Apolito, L.; Shen, S. Evaluation of Lithium Battery Cycle Aging Based on Temperature Increase During Charging. *Batteries* **2025**, *11*, 150. [CrossRef]
24. Zhang, Z.; Ji, C.; Liu, Y.; Wang, Y.; Wang, B.; Liu, D. Effect of aging path on degradation characteristics of lithium-ion batteries in low-temperature environments. *Batteries* **2024**, *10*, 107. [CrossRef]
25. Shao, D.; Hu, L.; Zhang, J.; Hu, R.; Zhang, G.; Jiang, L.; Wang, X.; Wen, Y. Advanced low-temperature preheating strategies for power lithium-ion batteries applied in electric vehicles: A review. *Int. J. Electrochem. Sci.* **2024**, *19*, 100817. [CrossRef]
26. Xiong, R.; Zhang, K.; Qu, S.; Tian, J.; Shen, W. A fast pre-heating method for lithium-ion batteries by wireless energy transfer at low temperatures. *eTransportation* **2023**, *16*, 100227.
27. Ren, X.; Sun, T.; Mao, S.; Zheng, Y.; Han, X.; Ouyang, M. Accelerated aging protocols design for Li-ion batteries based on equivalence of the degradation mechanisms. *J. Energy Storage* **2024**, *99*, 113386. [CrossRef]
28. Wang, M.; Wu, S.; Chen, Y.; Luan, W. The snowball effect in electrochemical degradation and safety evolution of lithium-ion batteries during long-term cycling. *Appl. Energy* **2025**, *378*, 124909. [CrossRef]
29. Kumar, K.; Rithvik, G.; Mittal, G.; Arya, R.; Sharma, T.K.; Pareek, K. Impact of fast charging and low-temperature cycling on lithium-ion battery health: A comparative analysis. *J. Energy Storage* **2024**, *94*, 112580. [CrossRef]
30. Guo, Y.; Cai, J.; Liao, Y.; Hu, J.; Zhou, X. Insight into fast charging/discharging aging mechanism and degradation-safety analytics of 18650 lithium-ion batteries. *J. Energy Storage* **2023**, *72*, 108331.
31. Gao, Z.; Xie, H.; Yang, X.; Niu, W.; Li, S.; Chen, S. The dilemma of c-rate and cycle life for lithium-ion batteries under low temperature fast charging. *Batteries* **2022**, *8*, 234. [CrossRef]
32. Wang, C.; Tang, Q.; Sun, T.; Feng, X.; Shen, K.; Zheng, Y.; Ouyang, M. Application of high frequency square wave pulsed current on lithium-ion batteries at subzero temperature. *J. Power Sources* **2025**, *633*, 236413. [CrossRef]